MArtian Radiation EnvIronment Experiment (MARIE)

Gautam D. Badhwar
Mail Code SN
Earth and Solar System Exploration Division
NASA Johnson Space Center, Houston, Texas 77058-3696
Phone: 281-483-5065 Fax: 281-483-5276 Email: Gautam.d.badhwar1@jsc.nasa.gov

Abstract

Space radiation presents a very serious hazard to the crews of interplanetary human missions. The two sources of this radiation are the galactic cosmic rays (GCR) and solar energetic particle (SEP) events. The GCR provides a steady source of low dose rate radiation that is primarily responsible for stochastic effects, such as cancer, and can also affect the central nervous system. The dose contribution is inversely correlated to the solar activity, the higher the activity the lower the dose rate. The SEP events, on the other hand, are directly correlated with solar activity, are a sporadic source of high dose rate radiation, which can lead to acute effects, such as nausea and even death. The radiobiological effectiveness (RBE) of GCR particles, due to the contribution of high charge (Z) component, is nearly twice as large as that from the solar events, which are mostly protons. Nuclear interactions of these components with the Martian atmosphere produce substantial flux of neutrons with high RBE. Because of the much higher energies of GCR particles compared to SEP, they are difficult to shield against, and for a given level of acceptable risk to the crew, small uncertainties in the knowledge of radiation received by the crew, lead to nearly exponential increase in the required shielding mass. The uncertainty in the knowledge of many fragmentation cross sections

and their energy dependence required by radiation transport codes, uncertainties in the ambient radiation environment, and knowledge of the Martian atmosphere, lead to large enough uncertainties in the knowledge of calculated radiation dose in both free space (cruise phase), in Martian orbit, and on Martian surface. Direct measurements of radiation levels, the relative contributions of protons, neutrons, and heavy ions, and Martian atmospheric characteristics is thus a pre-requisite for any human mission. A set of two spectrometers, one for the Lander and another for the Orbiter, were proposed for these studies. The Orbiter spectrometer is designed to measure the energy spectrum from 15 to 500 MeV/n, and when combined other space based instruments, such as the Advanced Composition Explorer (ACE), would provide accurate GCR spectra. Similarly, observations of solar energetic particles will be combined with observations at different points in the inner heliosphere from, for example, the Solar Heliospheric Observatory (SOHO), to gain information on the propagation and radial dependence in the Earth-Mars space. The Lander spectrometer was designed to measure the absorbed dose rate, dose equivalent dose rate, and the linear energy transfer (LET) spectra with the capability of separating the relative contribution of these quantities due to protons, neutrons, and high Z particles. However, since the Mars'01 Lander mission was dropped, such information cannot be obtained till some future flight. We plan to compare the Orbiter measurements with the best available radiation environment and transport models to both improve these models for subsequent use, and to provide key inputs for the engineering of required spacecrafts to better protect the human crews for interplanetary missions for space radiation. Studies of SEP events would be a critical part of the investigation.

Introduction

The two sources of radiation in free space, galactic cosmic rays, and solar energetic particles lead to different results of radiation effects. The steady low dose rate from GCR particles leads to stochastic effects and it is the long-term risk that is of main concern. Passage of heavy nuclei through the brain can lead to central nervous system (CNS) damage that may result, for example, in memory loss, and impact a human Mars mission. There are other effects, such as gastrointestinal, that are also of concern. The GCR contains fully stripped ions from hydrogen to uranium and span an energy range from ~ 1 MeV/n to 10^{20} eV. However, the flux of ions above nickel is too small to be of concern and energies above ~ 10 GeV/n do not contribute much to the radiation dose. The intensity of GCR is inversely related to solar activity, but this source of radiation is always present and because of the high energy of particles, difficult to shield against. Solar energetic particles (SEP) are sporadic events leading to sharp short-term increase in dose and dose rate. The Mars'01 mission will be launched around the peak of the current 24^{th} solar cycle. The analysis of previous SEP data (Feynman et al., 1990) shows that almost all of the SEP events fall about 3 years prior and 4 years past the solar maximum in the ~ 11 year solar cycle. Nymmik (1999) showed that the number of SEP events, N year, with a fluence, F, greater than 10^5 protons cm^{-2}, is given by: $N = 0.3W^{0.75}$, where W is the smoothed Wolf number. A number of events in the current solar cycle have been observed (November 1997, July 2000, and November 2000) in earth orbit and contributed to the exposure of the astronauts in the Mir and the International Space Station, where the earth's magnetic shielding provides a great reduction in radiation exposures. Such events would, of course, generate considerably higher doses in free space. There are no agreeable radiation exposure limits for interplanetary missions. Low-earth orbit (LEO) limits are given in Table 1 and are used

for guidance for Mars mission design studies. The stochastic limits are based on 3% excess mortality due to radiation.

Table 1: Recommended dose equivalent limits (Sv) for low-earth orbit flights (NCRP-98, 1989)

	BFO	Skin	Ocular lens
Career	1-4	6	4
Annual	0.5	3	2
30 day	0.25	1.5	1

These 1989 developed career limits are age and sex dependent. New recommendations from the National Council on Radiation Protection (Sinclair, 2000) would require lowering the career limits by factor of nearly 2, thus increasing the need for better dose estimation and radiation protection. The 30-day limits apply to SEP events.

Interest in the likelihood of a human Mars mission in the next decade has remained high. Studies on the radiation hazard of interplanetary missions were first carried out by Letaw et al. (1989) and the National Academy of Sciences (Stafford Report, 1993) reported that radiation protection posed a significant challenge to the design of such missions. With significant improvements in the development of models of the galactic cosmic radiation environment (Badhwar and O'Neill, 1996, Nymmik, 1996), improvements were made in predicting the dose rate during the cruise phase (Badhwar, 1994) using the NASA Langley Research Center developed radiation transport models BRYNTRN and HZETRN (Wilson, 1995). Simonsen et al., (2000) have, using improved version of these models, carried out more detailed analysis of expected dose rates for a potential Mars mission. Table 2 gives the surface exposure and shows that the dose equivalent is insensitive to the choice of the Mars atmospheric model.

Table 2: Martian surface radiation exposure at solar minimum.

Atmospheric Model	Overhead areal density ($g\ cm^{-2}$)	Annual Dose Equivalent (cSv)
COSPAR high density	21.9	9.00
Clancy	19.1	9.16
COSPAR Marsgram	17.3	9.30
COSPAR low density	16.0	9.43

A mission with a 1-year transit time and 1.5 year surface stay has been under consideration as a possible first human flight. Simonsen et al. using the recently developed concept of a lightweight inflatable habitable (TransHab) volume calculated the expected exposures on such a mission. Table 3 gives their results.

Table 3: Dose equivalent (cSv) estimates for a potential Mars mission. (Simonsen, 2000)

Source	1 yr Transit Dose Equivalent		1.5 yr Surface Dose Equivalent	
	Skin	BFO	Skin	BFO
Solar Maximum	33.4	27.0	20.1	17.6
Solar Minimum	93.8	72.7	46.5	40.7
August 1972 SEP	63.8	17.0	4.6	2.4

Uncertainties in the GCR model predictions and errors in the fragmentation cross-sections and their energy dependence directly impact the radiation dose and design of an appropriate shielding. A study by Badhwar et al., (1994) indicated that approximately 17.5 $g\ cm^{-2}$ of aluminum equivalent material would be sufficient to provide just enough shielding during a solar minimum transit phase to stay below the 50 cSv annual BFO limit. New calculations, however, with improved version of the HZETRN code show that almost 50 $g\ cm^{-2}$ is required for the same level of protection. This is due to the nearly asymptotic response of dose rate for large aluminum shielding thickness (Simonsen, 2000). Thus, the new challenge is to choose low atomic weight shielding materials and to significantly reduce the errors in estimating radiation exposures.

In estimating crew radiation exposures, the contribution of the secondary neutrons is currently not fully understood and not properly accounted for. This is a more serious problem with aluminum type shielding than with carbon based or more hydrogenated materials. It will definitely be of concern for a Lander mission due to production of neutrons in the Martian atmosphere and from the albedo neutrons. Since only an Orbiter instrument will be part of the Mars'01 mission, the focus will be to determine the galactic cosmic ray energy spectra during the maximum of the 24^{th} solar cycle, and study the dynamics of SEP events and their radial dependence, during the cruise phase and during the orbit phase around Mars.

Orbiter Instrumentation

Two flight instruments, one for the Orbiter and one for the Lander, based on a common design of the backplane, the central processing unit (CPU), power supply, and onboard data storage were designed and built. The Orbiter instrument consists of an energetic particle spectrometer that can measure the elemental energy spectra of charged particles of the energy range of 15-500 MeV/n. These limits are charge dependent and would extend to about 600 MeV/n for iron nuclei. The spectrometer is mounted on the science deck (Figure 1) with an angular acceptance of 50°. As the spacecraft orbits Mars, the axis of this field of view sweeps a cone of directions on the sky. During each orbit, the angle between the axis of the spectrometer's field of view and the mean interplanetary field direction varies from 90° to 180°.

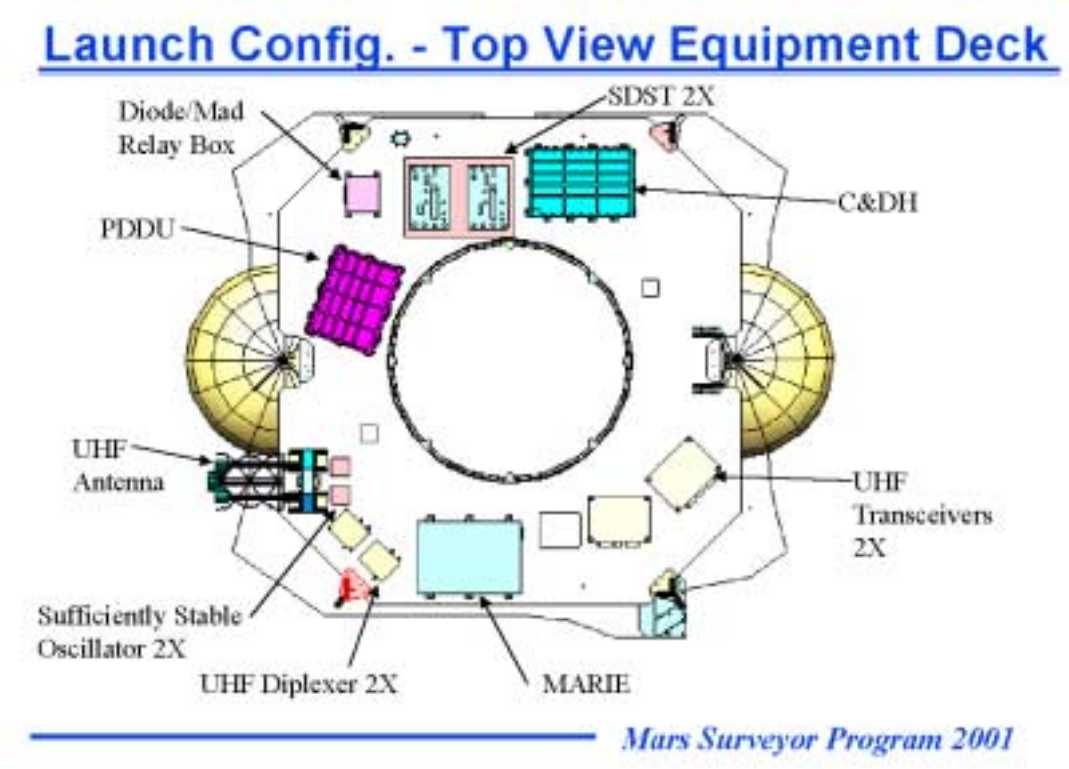

Figure 1: Location of MARIE at launch configuration

Figure 2 shows a schematic of the proposed spectrometer. It consists of a set of solid-state detectors and a high refractive index Cherenkov detector. The basic telescope geometry is defined by two 25.4 x 25.4 x 1 mm thick ion-implanted silicon solid-state detectors A1 and A2 that are operated at 160 V. In between A1 and A2 there are two 24 x 24 mm position sensitive detectors PSD1 and PSD2, each with a 24 x 24 mm wire grid, to define the incident direction of charged particle with respect to the axis of the telescope. The A2 detector is followed by a set of 5 mm thick lithium-drifted silicon solid-state detectors (B1, B2, B3, and B4), and a high refractive index Schot-glass Cherenkov (C) detector. The telescope is built like a personal computer. Each detector has its own card, with all of the electronics associated with the detector on it, including a 12-bit analog-to-digital (ADC) converter, and Field Programmable Gate Array (FPGA). The main power supply is a nominal 28 V (16 -32) DC Interpoint unit. There is

an 80 MB flash memory for data storage. The CPU board has an Intel microprocessor, and data communication hardware for transferring data through RS 422 and RS 232 ports. The memory device can store data for more than two weeks of operations. The instrument is a dE/dx x E telescope for stopping particles and dE/dx x C telescope for penetrating particles. Following coincidence rates are also recorded: A1A2, A1A2B1, A1A2B1B2, A1A2B1B2B3, A1A2B1B2B3B4, and A1A2B1B2B3B4C. The basic trigger is the A1A2 coincidence and requires a proton with energy >15 MeV. Following such a trigger all of the detectors are read out.

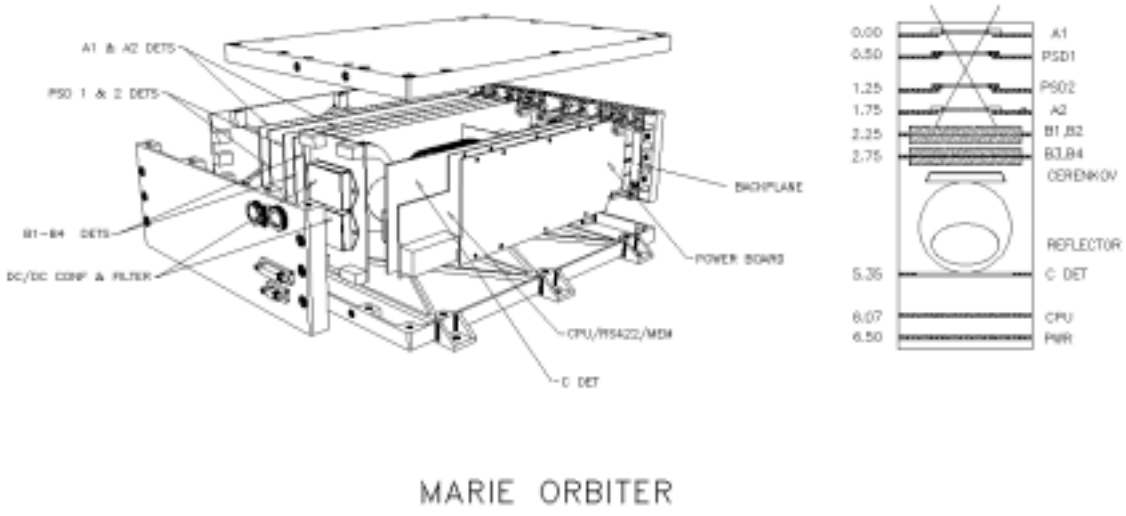

Figure 2: Schematic of Orbiter Spectrometer (Dimension in Inches)

Table 4 gives the area-solid angle product for various coincidence rates assuming an isotropic angular distribution of incident particles. Since the PSD detectors are slightly smaller than the trigger A detectors, about 15% of the particles miss these detectors and incident angle information for such events is lost. These detectors have separate thresholds for rows and columns.

Table 4: Area-solid product for an isotropic and sea-level muon angular distribution

Coincidence	Area-solid angle (cm^2 sr) – isotropic	Area-solid angle (cm^2 sr) –sea-level
A1A2	1.0	1.0
A1PSD1PSD2A2	0.85	0.85
A1A2B1	1.0	1.0
A1A2B1B2	0.996	0.997
A1A2B1B2B3	0.958	0.966
A1A2B1B2B3B4	0.907	0.922

If two wires have signals above the threshold, the position of each wire is noted; however, if more than two wires have signals above the threshold, only the median position of the wires is recorded. In addition, the magnitude of the total charge from the whole detector is read-out through a 10-bit ADC. Thus the PSDs not only provide the (x, y) coordinates of the passage of the particle through the detector, but a measure of the ionization loss in the detectors also. Figure 3 is an example of the angular distribution of sea-level muons measured by the telescope. Based on the 1 mm wire spacing and separation of the two detectors, the incident angle of the detector can be measured to better than $\pm$ 3%.

Figure 4 is a typical example of the pulse height distribution in various silicon detectors for sea-level muons. They have the characteristic Landau distribution. The width of the distribution arises from the quadratic sum of the detector noise, width due to fluctuations in the ionization energy loss, the Landau-Vavilov distribution, and due to the variation in path length in the detector.

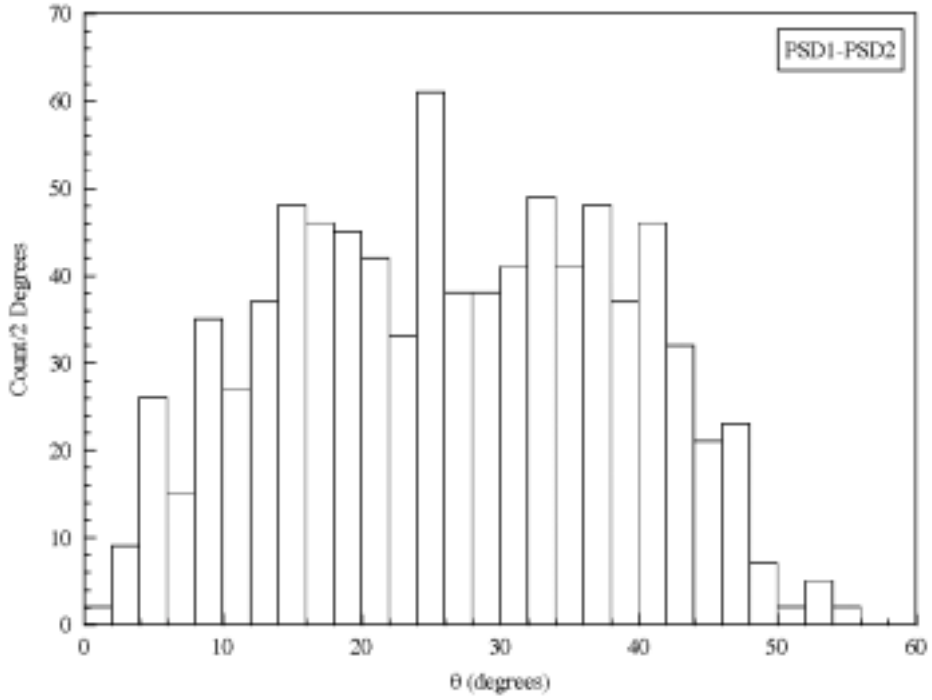

Figure 3: Comparison of the measured and expected muon angular distribution.

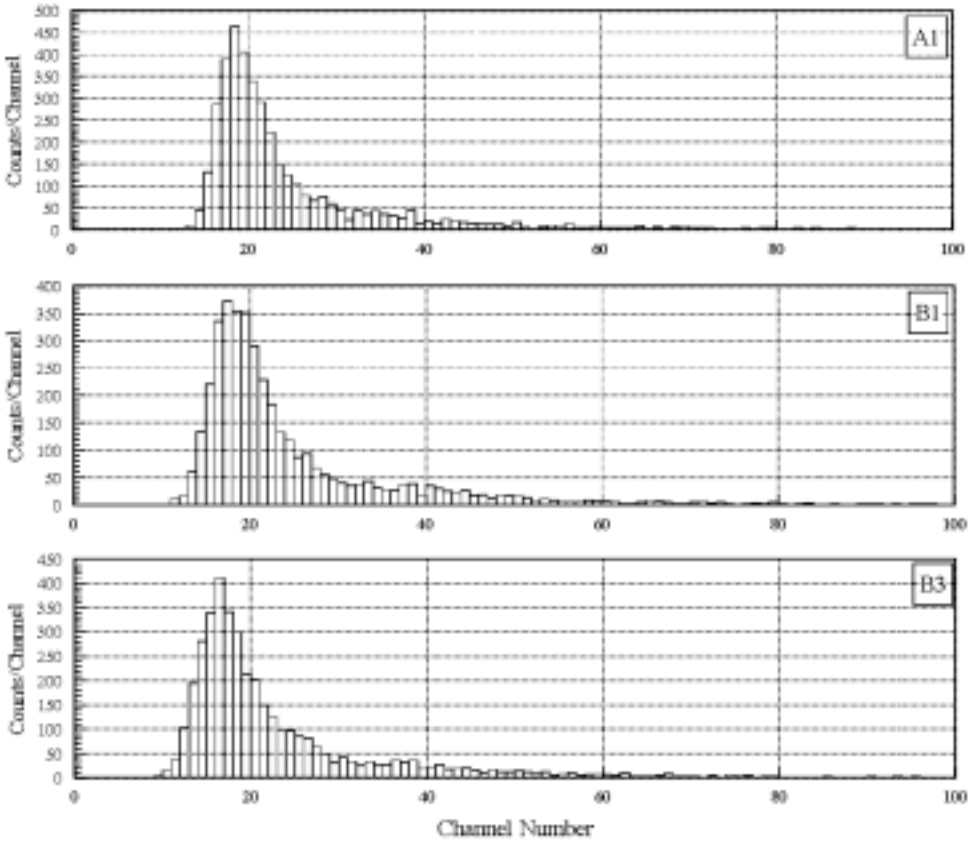

Figure 4: Typical pulse height spectra in three of the silicon detectors

Using the incident direction derived from the PSD detectors this data can be corrected for the acceptance angle leading to better charge and energy resolution. Figure 5 shows an example for the sea-level muons. The full width at half-maximum for Landau-Vavilov distribution would decrease approximately inversely as a function of increasing charge and would help in good overall charge resolution of the instrument.

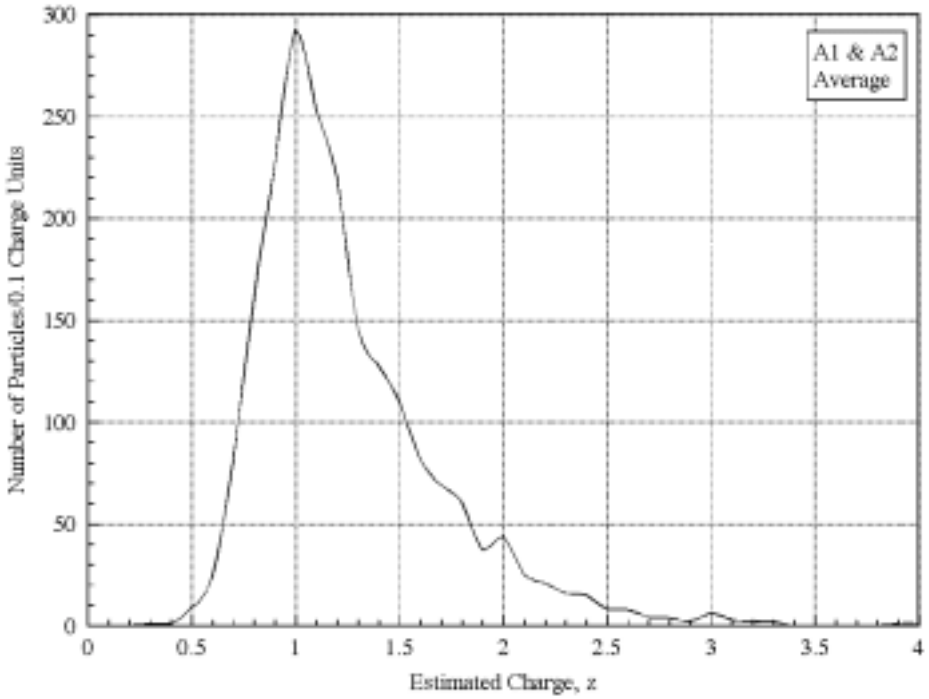

Figure 5: Calculated charge distribution using data for A1 and A2 detectors for muons (Z=1)

The dose, D, and dose equivalent, H, rates needed for astronaut exposures are given by:

$$D = (k/\rho) \int L\, J(L)\, dL$$

$$H = (k/\rho) \int L\, Q\,(L)\, J(L)\, dL$$

Here J(L) is the differential linear energy transfer (L ≡ dE/dx) spectrum of the incident particles, Q the definition of the radiation quality factor as a function of the linear energy transfer and multiplier for appropriate definition of the radiation units. Using the two trigger detectors A1 and A2 the LET distribution can be measured directly assuming that particles traverse the detectors at the mean incident angle. A more accurate distribution can be obtained using the knowledge of incident angles from the PSDs. Thus, direct information for the human exploration missions can be obtained if just the two trigger function normally. An example of the LET distribution measured with a silicon based LET spectrometer in a 51.65^{o} inclination orbit Space Shuttle flight (STS-91) around the time of solar minimum and comparison with HZETRN model calculations is shown in Figure 6.

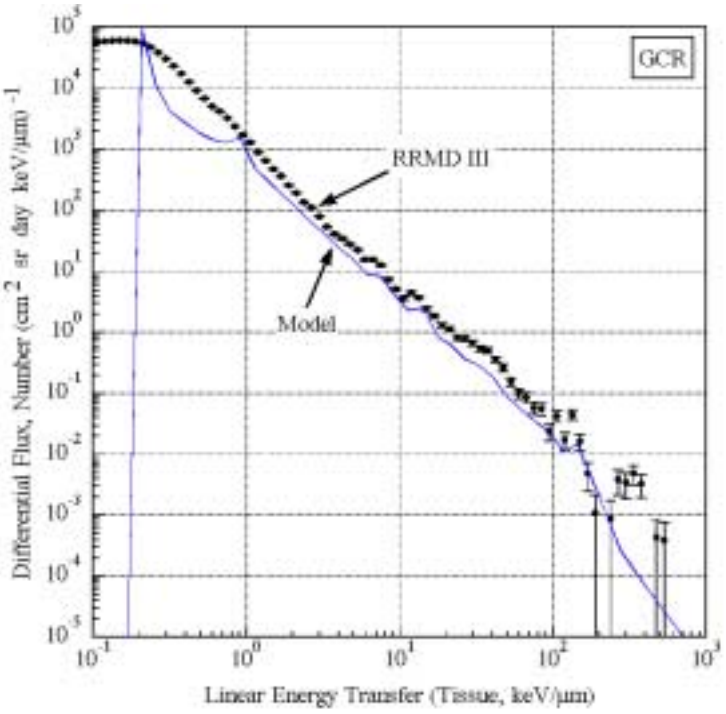

Figure 6: Measured LET spectra and comparison with HZETRN model calculations (GCR Component).

Also, using the knowledge of energy loss in all the detectors can determine the actual energy spectra and more accurate assessment by individual charges can be made.

Figure 7 plots the sea-level muon spectra in the Cherenkov detector, C, when the detector is accepting particles from the top and when the telescope has been inverted. Most of the photons coming out of the Schot-glass follow the direction of the incident particle. If the telescope is inverted, the photomuliplier tube can no longer view these photons. Thus the signal in C is very week. This provides an ability to distinguish the direction of the high-energy particles.

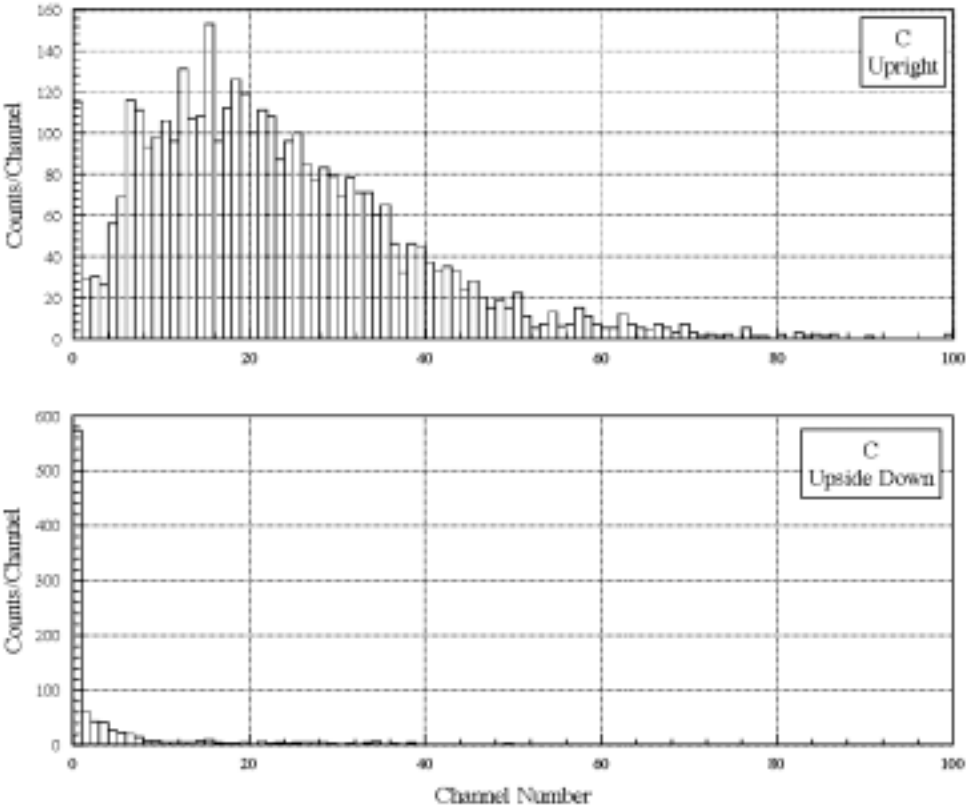

Figure 7: Pulse height spectra in Cherenkov detector in two orientations.

Data Analysis

Data from the spectrometer will be analyzed as follows. The data are divided into three energy regimes: (1) particles that stop in any detector from A2 to B4, (2) particles that go through B4 but do not give a Cherenkov signal, and (3) particles that give a Cherenkov signal. The angular information from the PSD detector would ensure that the particle falls in the right geometry.

Case 1: If the range energy relation for protons in silicon is expressed as a power law in energy with index, n, $R = K E^n$, and ΔE the energy loss in the thin detectors (A1 or A2). If E is the total energy deposited by the stopping particle, then

$$[\Delta E \times (E-\Delta E)] \propto (Z^2 M^{n-1})$$

where Z is the charge number and M is the mass of the incident particle, quantities that are element and isotope specific.

Thus, for each isotope, there exists a separate hyperbolic curve. Charge, mass and energy of the stopping particle can be determined. Figure 8 shows a plot of the energy loss in A1 versus the energy loss in A2 for protons and helium nuclei from the flight of a similar telescope (with no PSDs but an anti-coincidence counter).

Case 2: In this case, the particle energy is assumed to be greater than the energy required to penetrate all of the detectors but less than the Cherenkov threshold of ~ 180 MeV/n. The measurements of energy loss in each of the six (and in most cases eight) silicon detectors are compared with values calculated for a given energy. The energy is varied to find the best fit by minimizing the merit function:

$$\chi^2 (E) = \sum [\Delta E_i^{cal} - \Delta E_i^{obs}]^2$$

where i (=1,6) is the index for the detector and cal and obs refer to the calculated - and observed-energy loss.

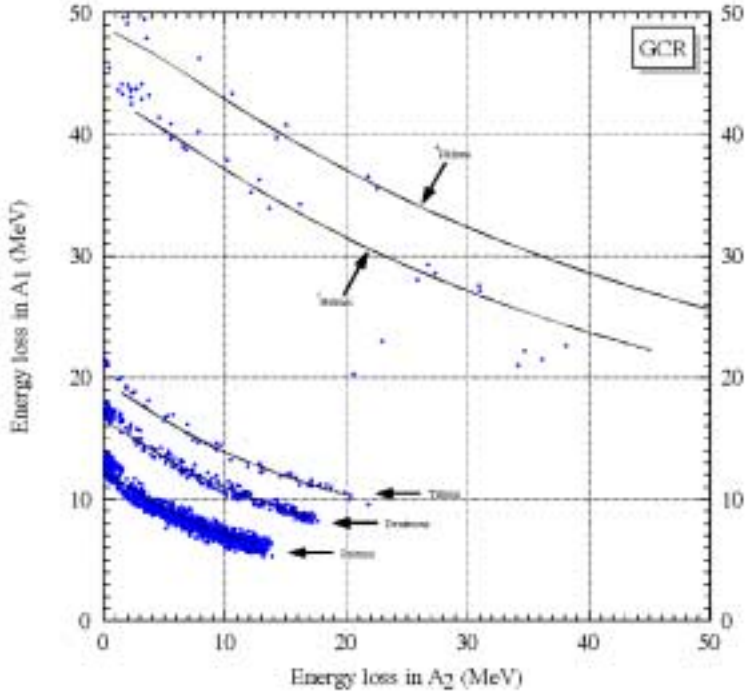

Figure 8: Energy loss curves determined for various particles

Case 3: In this case, the light emitted in the Cherenkov detector, C, is given by:

$$C = k\, Z^2 (1 - \beta_o^2/\beta^2)$$

where β_o is threshold velocity (=1/real part of index of refraction), and β is the particle velocity and the energy loss, ΔE, is

$$(\Delta E) \propto (Z^2/\beta^2)$$

These two equations are solved to obtain the charge and velocity (energy per nucleon). Using Schot-glass we can cover the energy range from about 180 MeV/n to 500 MeV/n.

Thus, this technique can cover the entire range from the minimum energy required to form the A1A2 coincidence, to the energy where the Cherenkov response saturates. In addition, one can construct an integral spectrum of SEP events, independently, from various coincident rates. An additional advantage of such an instrument is that using the energy loss in A1 and A2 and the angle of the incident particle, a *true* LET spectrum of particles can be determined.

The area solid angle of the proposed instrument would require large time integration. We plan to use our measurements of protons and helium GCR particles and correlate them with measurements from the ACE instrument (at L1) to obtain accurate GCR spectra in the Martian orbit.

These GCR spectra (which arrive isotropically) and the complete descriptions of the SEP events measured on the Orbiter are the input spectral functions to radiation transport models to predict the flux, dose, and LET spectra on the Martian surface. Because the arrival direction and distribution of SEPs can be measured, proper account can be taken of the shielding presented by the Martian atmosphere and the solid planet to different arrival directions. These predicted fluxes, doses and LET spectra can be compared with measurements made by a future Lander instrument to determine the radiation transport characteristics of the Martian atmosphere and provide key radiation information for both the cruise and landed phases of a future manned interplanetary mission. Excellent recent predictions have been recently reported by Wilson et al. (1999) and Reddy (1999).

Conclusion

The Orbiter spectrometer would provide data on GCR and SEP from the cruise phase to Martian orbit and in the Martian orbit. The information can be used for future human missions to Mars.

References

1. J. Feynman, T.P Armstrong, L. Dao-Gibner, and S. Silverman, New interplanetary proton fluence model. *J. Spacecraft* **27**, 403-410 (1990).

2. J.R. Letaw, R. Silverberg, and D.H. Tsao, Radiation hazards on space missions outside the magnetosphere. *Adv. Space Res.* **9**, 285-291 (1989).

3. G.D. Badhwar and P.M. O'Neill, Galactic cosmic radiation model and its applications. *Adv. Space Res.* **17**, 7-17 (1996).

4. G.D. Badhwar, F.A. Cucinotta, and P.M. O'Neill, An analysis of interplanetary space radiation exposure for various solar cycles. *Radiat. Res.* **138**, 201-208 (1994).

5. National Council on Radiation Protection and Measurements. Guidance on radiation received in space activities. Bethesda, MD: National Council on Radiation Protection and Measurements: NCRP Report No. 98, 1989.

6. W. K. Sinclair, Dose limits for astronauts, *Health Physics* **79**, 585-590 (2000)

7. J.W. Wilson, F.F. Badavi, F.A. Cucinotta, J.L. Shinn, and G.D. Badhwar HZETRN: description of a free-space ion and nucleon transport and shielding computer program. Springfield, VA: National Technical Information Service: NASA TP 3495: 1995.

8. L.C. Simonsen, J.W. Wilson, M.H. Kim and F.A. Cucinotta, Radiation exposure for human Mars exploration, *Health Physics* **79,** 515-525 (2000).

9. J.W. Wilson et al., Mars'01 symposium, USRA, Houston, Texas

10. R.C. Reddy, Mars'01 symposium, USRA, Houston, Texas

11. R.A. Nymmik, The problems of cosmic ray particle simulations for the near-Earth orbital and interplanetary flight conditions, *Rad. Meas.* **30**, 669-677 (1999).

12. Space Studies Board, National Research Council 1993, Scientific Prerequistes for Human Exploration, National Academy Press, Washington, D.C.